Edinburgh Research Explorer

Exploring the ATN classification system using brain morphology

Exploring the ATN classification system using brain morphology

Nils Heinzinger[1,2]*, Anne Maass[1,2], David Berron[1,2], Renat Yakupov[1,2], Oliver Peters[3,4], Jochen Fiebach[5], Kersten Villringer[5], Lukas Preis[4], Josef Priller[3,6,7,8], Eike Jacob Spruth[3,6], Slawek Altenstein[3,6], Anja Schneider[9,10], Klaus Fliessbach[9,10], Jens Wiltfang[11,12,13], Claudia Bartels[12], Frank Jessen[9,14,15], Franziska Maier[14], Wenzel Glanz[1], Katharina Buerger[16,17], Daniel Janowitz[17], Robert Perneczky[16,18,19,20], Boris-Stephan Rauchmann[18], Stefan Teipel[21,22], Ingo Killimann[21,22], Doreen Göerß[22], Christoph Laske[23,24], Matthias H. Munk[23,24], Annika Spottke[9,25], Nina Roy[9], Michael T. Heneka[9,10], Frederic Brosseron[9,10], Laura Dobisch[1], Michael Ewers[16], Peter Dechent[26], John Dylan Haynes[27], Klaus Scheffler[28], Steffen Wolfsgruber[9,10], Luca Kleineidam[9], Matthias Schmid[9,29], Moritz Berger[29], Emrah Düzel[1,2]†, Gabriel Ziegler[1,2]† and for the Alzheimer's Disease Neuroimaging Initiative

Abstract

Background The NIA-AA proposed amyloid-tau-neurodegeneration (ATN) as a classification system for AD biomarkers. The amyloid cascade hypothesis (ACH) implies a sequence across ATN groups that patients might undergo during transition from healthy towards AD: A−T−N− ➔ A+T−N− ➔ A+T+N− ➔ A+T+N+. Here we assess the evidence for monotonic brain volume decline for this particular (amyloid-conversion first, tau-conversion second, N-conversion last) and alternative progressions using voxel-based morphometry (VBM) in a large cross-sectional MRI cohort.

Methods We used baseline data of the DELCODE cohort of 437 subjects (127 controls, 168 SCD, 87 MCI, 55 AD patients) which underwent lumbar puncture, MRI scanning, and neuropsychological assessment. ATN classification was performed using CSF-Aβ42/Aβ40 (A+/−), CSF phospho-tau (T+/−), and adjusted hippocampal volume or CSF total-tau (N+/−). We compared voxel-wise model evidence for monotonic decline of gray matter volume across various sequences over ATN groups using the Bayesian Information Criterion (including also ROIs of Braak stages). First, face validity of the ACH transition sequence A−T−N− ➔ A+T−N− ➔ A+T+N− ➔ A+T+N+ was compared against biologically less plausible (permuted) sequences among AD continuum ATN groups. Second, we evaluated evidence

---

†Emrah Düzel and Gabriel Ziegler contributed equally to this work.

*Correspondence:
Nils Heinzinger
nils.heinzinger@st.ovgu.de
Full list of author information is available at the end of the article

Heinzinger *et al. Alzheimer's Research & Therapy*   (2023) 15:50

Page 2 of 18

for 6 monotonic brain volume progressions from A−T−N− towards A+T+N+ including also non-AD continuum ATN groups.

Results The ACH-based progression A−T−N−➔A+T−N−➔A+T+N−➔A+T+N+ was consistent with cognitive decline and clinical diagnosis. Using hippocampal volume for operationalization of neurodegeneration (N), ACH was most evident in 9% of gray matter predominantly in the medial temporal lobe. Many cortical regions suggested alternative non-monotonic volume progressions over ACH progression groups, which is compatible with an early amyloid-related tissue expansion or sampling effects, e.g., due to brain reserve. Volume decline in 65% of gray matter was consistent with a progression where A status converts before T or N status (i.e., ACH/ANT) when compared to alternative sequences (TAN/TNA/NAT/NTA). Brain regions earlier affected by tau tangle deposition (Braak stage I-IV, MTL, limbic system) present stronger evidence for volume decline than late Braak stage ROIs (V/VI, cortical regions). Similar findings were observed when using CSF total-tau for N instead.

Conclusion Using the ATN classification system, early amyloid status conversion (before tau and neurodegeneration) is associated with brain volume loss observed during AD progression. The ATN system and the ACH are compatible with monotonic progression of MTL atrophy.

Trial registration DRKS00007966, 04/05/2015, retrospectively registered.

Keywords MRI, Alzheimer's disease, Memory, Voxel-based morphometry, VBM, ATN, Biomarker, Amyloid

Introduction

Alzheimer's disease (AD) is a slowly evolving neurodegenerative condition where initial brain changes can be found up to decades before the clinical onset and ultimately result in progredient cognitive decline and brain atrophy often studied with magnetic resonance imaging (MRI) [1–3].

AD is characterized by the accumulation of protein deposits, i.e., β-amyloid plaques and neurofibrillary tangles (NFT) consisting of hyperphosphorylated tau which can be assessed using cerebrospinal fluid (CSF) biomarkers [4, 5]. A reliable marker reflecting amyloid deposition is the Aβ42/Aβ40 ratio which decreases with increasing deposition [6]. Accumulation of tau tangles is mirrored by increasing CSF hyperphosphorylated tau, while CSF total tau has been more generally associated with neuronal loss, not necessarily AD specific. Those biomarkers have shown potential for predicting the clinical diagnostic conversions [7–9] and worsening of memory performance during disease progression [10].

One key concept about the disease progress and pathological timeline has been introduced as the amyloid cascade hypothesis (ACH) [1, 11–13]. Due to different predispositions, including age [14], genes [15], or vascular risk factors [16], ß-amyloid is increasingly formed from precursor proteins which leads to its aggregation in the brain. Then, ß-amyloid can induce hyperphosphorylation and malformation/misfolding of intracellular tau proteins, which aggregate in forms of NFTs [13]. Increased cellular stress results in neuronal loss which typically manifests behaviourally in progressive cognitive decline. Neuronal death in AD manifests in a typical MRI atrophy pattern with strongest morphometrical changes situated in medial temporal lobe (MTL) and other limbic regions, while the primary motor and sensory cortex are often spared [17, 18]. Although the ACH was postulated about 30 years ago, the hypothesis is still under refinement and critical review [13, 19, 20]. Moreover, the stereotypical progression pattern of tau/NFT spread from the transentorhinal region via the limbic system to the whole cortex during AD progression can be classified into six Braak stages, which have been first described in an autopsy study [5], and later tested in positron emission tomography studies [21, 22] or VBM atrophy studies [23].

Recently, a new descriptive ATN classification for AD which emphasizes pathological and physiological rather than traditional clinical measures such as neuropsychological test scores was proposed [24, 25]. In the ATN system, for the three binary categories amyloid burden, tau burden, and neurodegeneration, subjects are rated as normal (physiological, "−") or abnormal (pathological, "+"). The resulting 8 (=2^3) groups with different biomarker combinations range from A−T−N− (suggesting no pathology) to A+T+N+ (with pathology in all categories). It has been suggested that all ATN biomarker combinations with A+ reflect a pathological change related to the AD continuum. Several recent studies explored the prognostic possibilities for clinical progression and cognitive decline using ATN [26–30]. However, while the ATN classification does not directly imply a progression cascade or a set of subsequently following stages per se, it may be used for this particular purpose. For example, the sequence of a disease transition across pathology groups (1) A−T−N− (2) A̲+T−N− (3) A+T̲+N− (4)

A+T+$\underline{N+}$ is more compatible with the amyloid cascade hypothesis than other progression sequences based on ATN classification groups [25]. If individual participants follow this particular disease progression profile, this would imply a monotonic volume loss across groups (1)➔(2)➔(3)➔(4) in brain areas associated with AD. While above progression sequence is partially supported in selected studies [31, 32], those findings are limited to recordings of non-imaging between-group biomarker differences. Although there is evidence for deviating sequences of progression [32], studies focusing on local voxel-based anatomical analysis in relation to ATN groups are still missing (see, e.g. [33]).

Here we study whether above progression implied by the ACH is reflected in specific patterns of local GM volume decline using cross-sectional data from a large neuroimaging cohort (DELCODE; DZNE Longitudinal Cognitive Impairment and Dementia Study) which is well characterized by CSF biomarkers. The DELCODE cohort is specifically enriched in subjects that are at risk for developing AD such as subjective cognitive decline (SCD), but also mild cognitive impairment (MCI) and thus more likely comprises individuals in early preclinical stages of AD (A+).

GM volume is a sensitive marker for local brain changes or pathological processes. As this marker is continuous, smallest substance differences for all brain regions can be measured and intermediate changes are detectable even when they would not cause an ATN status conversion. We hypothesize that GM in the hippocampal-network decreases following the ACH sequence and (1) test face validity of an ACH-based sequence using voxel-based morphometry without a priori regional assumptions; and (2) compare the evidence for volume loss reflecting the ACH sequence in comparison to other biologically possible progressions outside the AD continuum. Finally, the concordance between ACH progress and Braak staging is evaluated. We expect earlier Braak stages to be stronger affected by atrophy during the ACH sequence. It might occur that the volume alteration is regionally modulated by, e.g., reserve mechanisms. Since operationalization might be crucial, we also evaluate the impact of alternative choices for dichotomization of the N category using both t-tau or hippocampal volume.

Methods

Study design and participants

This study uses the baseline data of the DELCODE cohort, an observational multicentre study with 10 sites from the German Centre of Neurodegenerative Diseases (DZNE). Its focus is the multimodal assessment of preclinical stages of dementia of Alzheimer's type (DAT) including SCD, MCI, DAT, and DAT

relatives [34]. While SCD, MCI, and DAT participants were recruited from memory clinics, relatives of DAT patients and healthy controls were recruited by advertisement and initially screened per phone for self-experienced cognitive decline and memory worries. Further SCD inclusion criteria were a normal cognitive performance (specified as within 1.5 SD compared to an age, sex, and education years adjusted control group) in all subtests of the CERAD-plus battery and a MMSE score between 26 and 30 and a CDR score ≤ 0.5.

Participants with MCI were below 1.5 SD in the CERAD-plus battery, but did not fulfil dementia criteria of NINDCS/ADRDA [35]. Subjects diagnosed as DAT were fulfilling NINDCS/ADRDA criteria, have a CERAD-plus score of below 1.5 SD, and were within an extended MMSE score range of 18–26 and have a CDR rating of ≥ 1. DAT relatives have a first-grade sibling with diagnosed DAT and do not fulfil MCI or DAT criteria.

Noncomplaining healthy controls (NC) neither suffered from subjective or objective cognitive impairment. All participants were native German speakers, older than 60 years, and gave written informed consent and had a study partner available for consultation. Other neurological or psychiatric disorders than DAT were excluded. More information on study design and inclusion/exclusion criteria can be found elsewhere [34]. DELCODE is retrospectively registered at the German Clinical Trials Register (DRKS00007966), (04/05/2015) and was approved by ethical committees and local review boards. Of a total of 1079 participants at baseline timepoint, we finally included 437 subjects with available quality checked MRI imaging and CSF biomarkers (see below). Based on a clinical classification approach, this includes 127 NC (including DAT relatives), 168 SCD, 87 MCI, and 55 DAT patients. A summary of demographic information of the analyzed sample is provided in results Table 1.

Neuropsychological testing

In DELCODE, subjects underwent a large battery of neuropsychological tests. Due to our focus on global cognition and memory aspects in healthy and (pre-) clinical DAT patients, we use the Mini-Mental State Examination (MMSE, [36]) and a reliable memory composite factor score (further denoted as memory performance). This score was created by confirmatory factor analysis and enables detecting subtle cognitive deviations in SCD when compared to NC subjects [37].

Biomarker and MRI data acquisition

Lumbar puncture was carried out by trained study assistants in 49% of DELCODE participants. CSF samples

Heinzinger *et al. Alzheimer's Research & Therapy* (2023) 15:50

Page 4 of 18

Table 1 DELCODE sample characteristics and ATN group classification

ATN groups	Normal	Non-AD pathologic change			Alzheimer's continuum groups			
	A−T−N−	A−T−N+	A−T+N−	A−T+N+	A+T−N−	A+T−N+	A+T+N−	A+T+N+
Group size	143	41	29	14	45	23	61	81
Age (years) mean (SD)	69.64 (5.50)	68.10 (5.85)	70.20 (4.56)	70.86 (5.90)	69.97 (5.12)	70.91 (7.10)	73.20 (5.30)	73.46 (5.84)
Sex (% female)	48.25%	48.78%	72.41%	28.57%	42.22%	39.13%	47.54%	55.56%
Education years mean (SD)	14.65 (2.92)	14.71 (2.87)	13.79 (2.02)	16.57 (2.53)	14.07 (2.53)	14.43 (3.19)	13.67 (3.33)	13.75 (2.98)
MMSE mean (SD)	29.15 (1.19)	28.54 (1.98)	29.14 (1.27)	29.14 (1.61)	29.24 (0.77)	27.52 (3.29)	27.52 (3.06)	26.12 (3.23)
Memory performance mean (SD)	0.39 (0.51)	0.13 (0.84)	0.42 (0.67)	0.01 (0.99)	0.35 (0.64)	−0.52 (1.05)	−0.44 (1.09)	−1.18 (1.00)
CSF Aβ42/40 mean (SD)	0.110 (0.011)	0.108 (0.011)	0.112 (0.013)	0.118 (0.014)	0.074 (0.012)	0.064 (0.015)	0.053 (0.011)	0.050 (0.013)
CSF phospho-tau (pg/ml) mean (SD)	41.02 (8.81)	39.85 (11.84)	68.02 (10.88)	74.68 (19.41)	41.88 (9.99)	44.49 (9.40)	93.26 (50.38)	95.06 (31.09)
CSF total tau (pg/ml) mean (SD)	288.18 (89.16)	291.24 (131.09)	465.98 (115.59)	544.38 (167.71)	321.41 (104.50)	312.96 (94.48)	677.41 (335.83)	778.43 (287.03)
aHV (ml) mean (SD)	3.14 (0.21)	2.64 (0.15)	3.18 (0.24)	2.63 (0.11)	3.12 (0.21)	2.60 (0.21)	3.12 (0.23)	2.56 (0.22)
WMH (ml) mean (SD)	3.29 (5.31)	3.27 (6.07)	1.42 (1.70)	2.09 (2.83)	3.19 (3.61)	4.66 (6.05)	6.99 (11.61)	6.34 (7.96)

Overview of descriptive characteristics of the DELCODE sample and ATN group statistics. *Non-AD pathologic change* ATN groups that are related to neuronal conditions other than AD, *Alzheimer's continuum groups* Aβ-positive groups that are related to AD

aHV adjusted hippocampal volume, *WMH* white matter hyperintensities

were centrifuged, aliquoted, and stored at −80°C for retests. Biomarkers known to be related to AD pathology (CSF Aβ42, total tau, hyperphosphorylated tau) were determined by commercially available kits (V-PLEX Aβ Peptide Panel 1 (6E10) Kit (K15200E), V-PLEX Human Total Tau Kit (K151LAE) (both Mesoscale Diagnostics LLC, Rockville, USA), Innotest Phospho-Tau(181P) (81581; Fujirebio Germany GmbH, Hannover, Germany)).

MRI scans were acquired in 9 out of 10 involved DZNE sites (3T Siemens scanners: 3 TIM Trio systems, 4 Verio systems, 1 Skyra and 1 Prisma system). Our main analyses were based on whole brain T1-weighted MPRAGE (3D GRAPPA PAT 2, 1 mm³ isotropic, 256 X 256 px, 192 slices, sagittal, ~5 min, TR 2500 ms, TE 4.33 ms, TI 110 ms, FA 7°). Further ROI and covariate processing was based on additionally available FLAIR and T2-weighted protocols (for details see [34]). Additional details on standard operation procedures, quality assurance, and assessment (QA), performed by the DZNE imaging network (iNET, Magdeburg), can be found elsewhere [34].

Image processing and computational brain morphometry

The MPRAGE images were processed using SPM (SPM12 v7771, Statistical Parametric Mapping software;

Wellcome Trust Centre for Human Neuroimaging, London, UK, [38]) and CAT-Toolbox (CAT12.6 r1450, Structural Brain Mapping group, Jena University Hospital, Jena, Germany, [39]) under MATLAB (r2019b, The MathWorks, Inc., Natick, Massachusetts, USA). As first step, a correction for field inhomogeneities was applied. Then the images were segmented into GM, WM, and CSF maps using CAT which includes a partial volume estimation correction on AMAP approach [40]. The received tissue maps with a 1-mm isometric voxel size are warped to a study-specific template in MNI space using Geodesic Shooting approach [41]. The GM tissue maps were modulated by the Jacobian determinant to enable voxel-based comparisons of local gray matter volume across subjects. We tested the impact of different Gaussian blurring kernels on the model and finally opted for a kernel with 6 mm full width half maximum (FWHM). The impact of Gaussian blurring with different FWHM kernel sizes on the model can be found in the supplement (Supplemental File 1). The resulting tissue maps were quality tested using CAT's sample homogeneity check and 15 subjects were excluded due to preprocessing artifacts.

For complementary ROI analysis, we used Freesurfer's (v6.0, [42]) volume reconstruction (cortical stream [43], subcortical stream [44]) to extract region

of interest volumes. This was carried out by the default pipeline initiated by a "recon-all -all" command which contains all preprocessing steps needed, including for example intensity normalization, surface registration to Talairach space, skull stripping, subcortical segmentation and calculation of affiliated region statistics, WM segmentation, tessellation and inflation of pial parcellated WM surfaces, and cortical parcellation with calculation of cortical region statistics. Four ROIs (amygdala, hippocampus, entorhinal cortex, precuneus), well known to be affected early by AD pathology, were assessed [17, 45–48]. Furthermore, anatomical masks representing Braak stages were created following [49] and warped to MNI space. Thus, the following cortical regions were included as aggregated volumes: stage I/II: entorhinal cortex and hippocampus, stage III/IV: limbic, insular and temporal regions, V/VI: remaining cortical regions including primary sensory/motor areas or precuneus.

In order to enable a reliable operationalization of the N category of ATN system, we used the specifically developed hippocampal segmentation in Freesurfer that is based on a high-resolution T2-weighted scan of the medial temporal lobe [50]. Note, that the obtained hippocampal volumes were only used for the ATN classification of each participant, while all presented voxel-based and ROI volumes were based on conventional CAT and Freesurfer segmentations (as dependent variable). A strong co-occurrence of AD and white matter hyperintensities (WMH) as sign of vascular damage has been reported [16, 51–54]. To account for WMH during our analyses, the total lesion volume was extracted using Lesion segmentation toolbox (v3.0.0, LPA and an 0.5 binary threshold, [55, 56]).

ATN classification and group comparison

Each participant was classified as normal (−) or abnormal (+) in the amyloid (A) and tau (T) category depending on their biomarker levels of Aβ42over40 and phospho-tau181 respectively. Cutoffs were estimated by a ROC analysis and Youden's index (A = 0.09, T = 57 pg/ml, [34]). In this study, we explored effects of two different choices for the neurodegeneration (N) category. We focused on (1) adjusted hippocampal volume (denoted as aHV; cutoff = 2821.1 μl) and (2) CSF total tau (cutoff = 470 pg/ml). aHV was derived from the Freesurfer segmentation (see above) and corrected for age, sex, education, total intracranial volume (TICV), and WMH using a linear regression model. Dichotomization of participants' aHV into N− and N+ was performed using Gaussian mixture modelling (GMM) similar to established cutoff estimation for CSF biomarkers used for the A and T category [57].

To assess group differences in age and education, one-way ANOVAs with ATN status as between-subject variable were used. Group differences in cognition (MMSE and memory performance) were tested in ANCOVAs with ATN status as between-group variable and age, sex, and education as covariates. In all cases, post hoc analysis was performed by two sample *t*-tests using a Bonferroni correction to account for multiple comparisons. Notably, analyses were restricted to the four groups of the ACH-based progression (1) A−T−N− (2) A̲+T−N− (3) A+T̲+N− (4) A+T+N̲+ since we focused on implications for common AD-related trajectories. The distribution of ATN status per clinical diagnosis was tested by 2-sided Fisher's exact test for distribution differences between cognitively unimpaired (NC, SCD) and cognitively impaired (MCI, DAT) subjects. Significance level is set to $p < .05$ (*) or $p < .001$ (**) respectively.

Testing the evidence for a monotonic decrease of brain volume over ATN progression groups

We aimed to test the evidence of local brain GM volume loss as a process of AD progression. As predicted by the ACH, the volume would decline over the following groups (1) A−T−N− (2) A̲+T−N− (3) A+T̲+N−; to (4) A+T+N̲+. Thus, we hypothesized later ATN stages to be associated with significantly reduced GM in AD-related areas. We estimated a voxel-wise general linear model describing the local GM volume *y* for the 4 given groups as

$$y = X\beta + \epsilon$$

with design matrix *X*, coefficients *β*, and residuals *ε*. The design matrix was chosen to define β_1 as group mean of the first group, and for *g=2,3,4* coefficient β_g as group difference of group *g* and *g-1*. The model was fitted under linear constraints that $\beta_g \leq 0$ for *g=2,3,4* and therefore implementing a monotonic decline of volume across groups *1* to *4* (using MATLAB R2019b's function for constrained optimization lsqlin). For instance, if a voxel has a true monotonic decline of volume *y* over groups *1,2,3,4*, the model evidence is expected to be higher than for an alternative model with reversed group order, e.g., *4,3,2,1*. We further compared different hypothesized and alternative sequences of volume decline progressions using the Bayesian Information Criterion [58] (BIC) which compares the likelihood how well the data is described using a monotonic function while accounting for model complexity (Fig. 1).

First, face validity of the ACH hypothesis was tested by comparing the evidence of the above ACH-based sequence (1) ➔ (2) ➔ (3) ➔ (4) against 23 (=4*3*2*1-1) alternative monotonic progressions generated by permutation which are a priori less plausible if ACH is

Heinzinger *et al. Alzheimer's Research & Therapy*   (2023) 15:50

Page 6 of 18
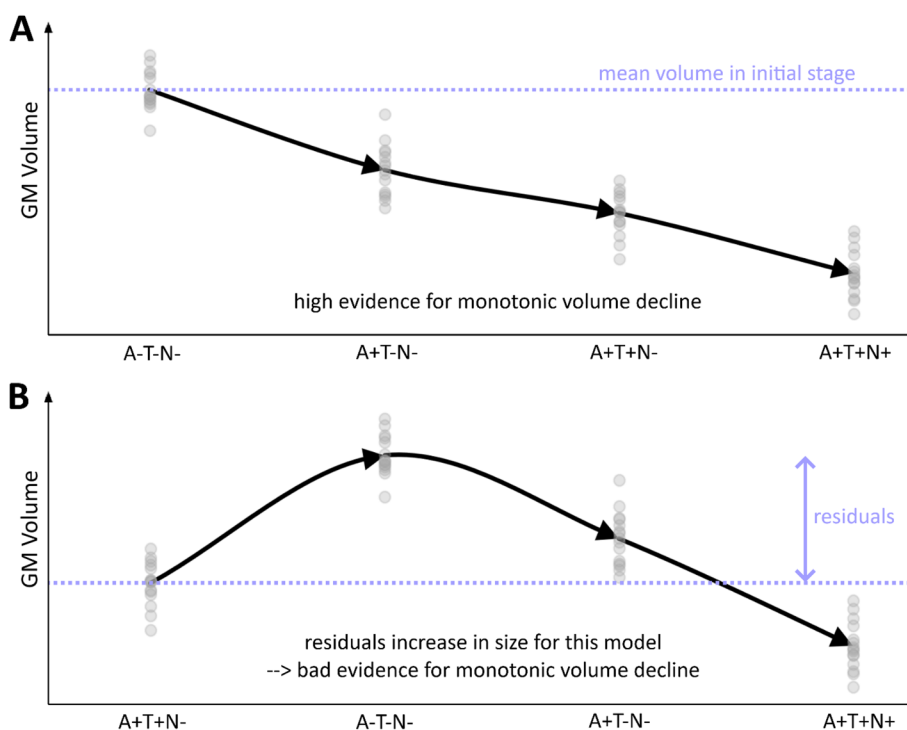
Fig. 1 Monotonic and non-monotonic volume decline using ATN. **A** An illustration of monotonic GM volume decline as hypothesized when following the ACH hypothesis using ATN groups. **B** A permutated order of the upper case that clearly not shows a monotonic volume decline. A temporary volume increase causes large residuals that cannot be explained by a monotonic model. Therefore, the pathway in **A** would be preferred over **B** ("higher evidence for monotonic decline in **A**")

true. Note that this analysis was restricted to 4 primarily AD-related of all 8 possible ATN classification groups, where it is assumed that amyloid conversion happens before status conversion of tau and neurodegeneration. In a second analysis, the evidence of the ACH-related volume trajectory was compared against 5 biologically plausible alternative sequences including also ATN groups which are considered outside the AD continuum, in particular ANT (i.e., amyloid-conversion first, N-conversion second, tau-conversion last; therefore "ANT"), TAN, TNA, NAT, and NTA. These 6 sequences represent all conceivable possibilities to convert in three steps from A−T−N− (no pathology) to A+T+N+ (full pathology).

In this study, all tests were performed both on (A) whole brain voxel-based modulated GM volume images and (B) a priori hypothesized ROIs. Voxel-based tests were restricted to GM using an absolute threshold of .05. In addition, the percentage of voxels with the highest evidence for the ACH trajectory inside every ROI mask is provided.

All statistical analyses were performed in MATLAB. Voxel-wise test results are presented as maps with the highest evidence for one particular model and log p maps for inference on statistical parameters such as successive

volume decline over groups (using FDR correction for multiple comparisons, $p<0.05$). Finally, the percentage of GM voxels with the highest evidence for a certain progression sequence is provided. All analyses were accounting for covariates age, sex, education, TICV, and WHM. All main results are reported for N operationalized by aHV and selected results using CSF total tau can be found in the Supplementary material.

Model verification using an ADNI dataset

We additionally aimed to support the validity of our ROI-modelling results by out-of-sample replication using the Alzheimer's Disease Neuroimaging Initiative [59]. The ADNI was launched in 2003 as a public-private partnership, led by Principal Investigator Michael W. Weiner, MD. The primary goal of ADNI has been to test whether serial MRI, positron emission tomography, other biological markers, and clinical and neuropsychological assessment can be combined to measure the progression of MCI and early AD. For up-to-date information, see [59].

The analyzed subsample for out-of-sample replication encompasses 285 subjects from ADNI2 (68 NC, 34 SCD, 169 MCI, 14 AD) which had Freesurfer (v5.1, [42]) volumes and CSF biomarkers available. ATN dichotomization was performed using CSF Aβ42, CSF p-tau, and aHV

generated by Freesurfer's hippocampal subfield segmentation. Cutoffs were estimated using GMM. We focused on ROI volumes of amygdala, hippocampus, entorhinal cortex, precuneus, and aggregated Braak stages and again tested the face validity of the ACH against 23 permutations of ATN groups as well as compared the ACH against five other progressions towards AD after correction for age, sex, education, TLV, and TICV as described above (for DELCODE).

Results

Sample demographics and ATN group comparisons

Key characteristics of the analyzed DECLODE sample are summarized in Table 1, and selected comparisons (Bonferroni) can be found in Fig. 2. As expected, we found that age differed across ATN groups ($F_{(7,429)} = 6.65$, $p < .001$). ATN groups showed also differences in years of education ($F_{(7,429)} = 2.63$, $p < .05$). With respect to cognition, we found a significant effect of ATN group ($F_{(7,426)} = 13.46$, $p < .001$), age ($F_{(1,426)} = 14.78$, $p < .001$), and education ($F_{(1,426)} = 19.58$, $p < .001$) on MMSE scoring, but no effect of sex ($F_{(1,426)} = 0.93$, $p = .33$). Similar results were obtained for the memory performance, where ATN status ($F_{(7,426)} = 28.10$, $p < .001$), age ($F_{(1,426)} = 44.54$, $p < .001$), education ($F_{(1,426)} = 39.78$, $p < .001$), and sex ($F_{(1,426)} = 3.87$, $p < .05$) were significant.

As shown in Fig. 2, the age increased while global cognition (MMSE) and memory performance decreased following a hypothesized disease progression using the ACH sequence (A−T−N− ➔ A+T−N− ➔ A+T+N− ➔ A+T+N+). No systematic pattern was found for years of education. These effects could be reproduced using CSF total tau for N (Supplemental File 2).
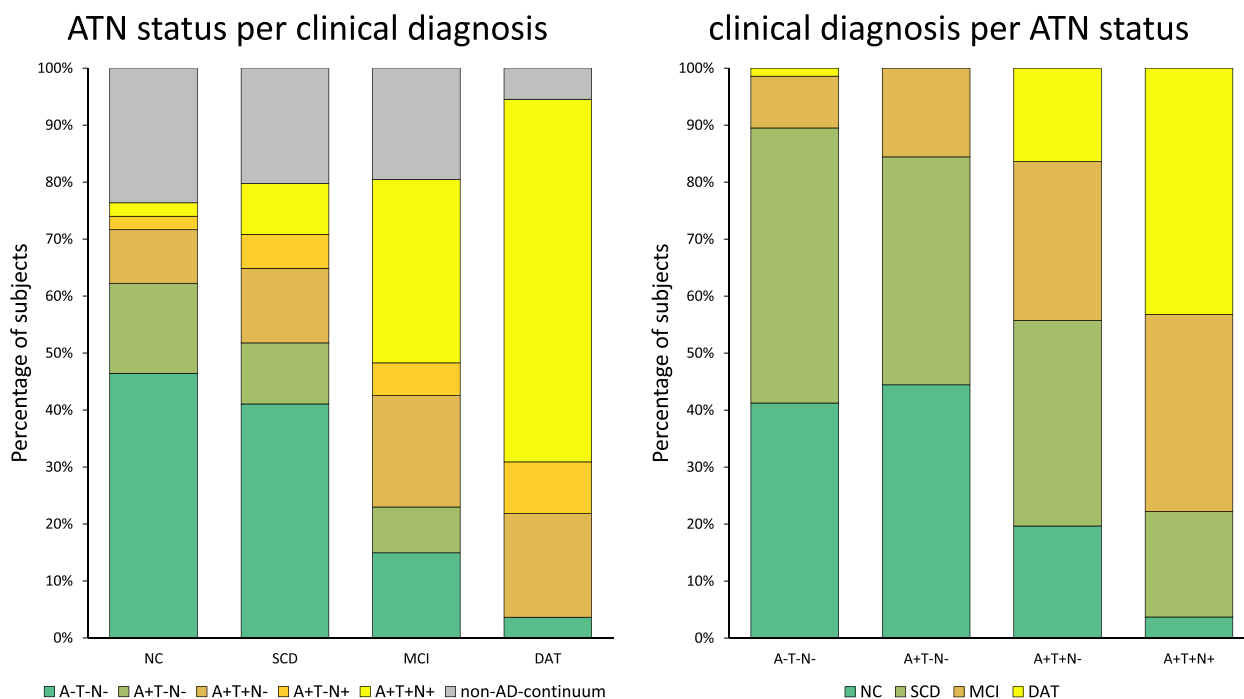
Association of ATN status and clinical diagnosis

We observed an association of the ATN status and clinical diagnosis groups comparing cognitively unimpaired (NC, SCD) and cognitively impaired (MCI, DAT) participants for A−T−N− ($p < .001$), A−T+N− ($p < .05$), A+T−N− ($p < .05$), A+T+N− ($p < .05$), and A+T+N+ ($p < .001$). No non-random association was found for A−T−N+ ($p = .49$), A−T+N+ ($p = .40$), and A+T−N+ ($p = .26$). Compared to A−T−N−, the highest relative risk for DAT was found in A+T+N+ (30.90 times higher) and A+T−N+ (15.54 times). The lowest risk for DAT relative to A−T−N− was in A−T+N− (2.47 times higher), while no DAT cases were recorded in A−T+N+ or A+T−N−. Results suggested that more impaired clinical groups, especially DAT, were found more often among the Alzheimer's continuum ATN groups (i.e., in A+), while cognitively unimpaired status was rather associated to no brain pathology (i.e., A−T−N−). For percentual distribution, see Fig. 3. A similar pattern was observed for N measured by CSF total tau (Supplemental File 3).
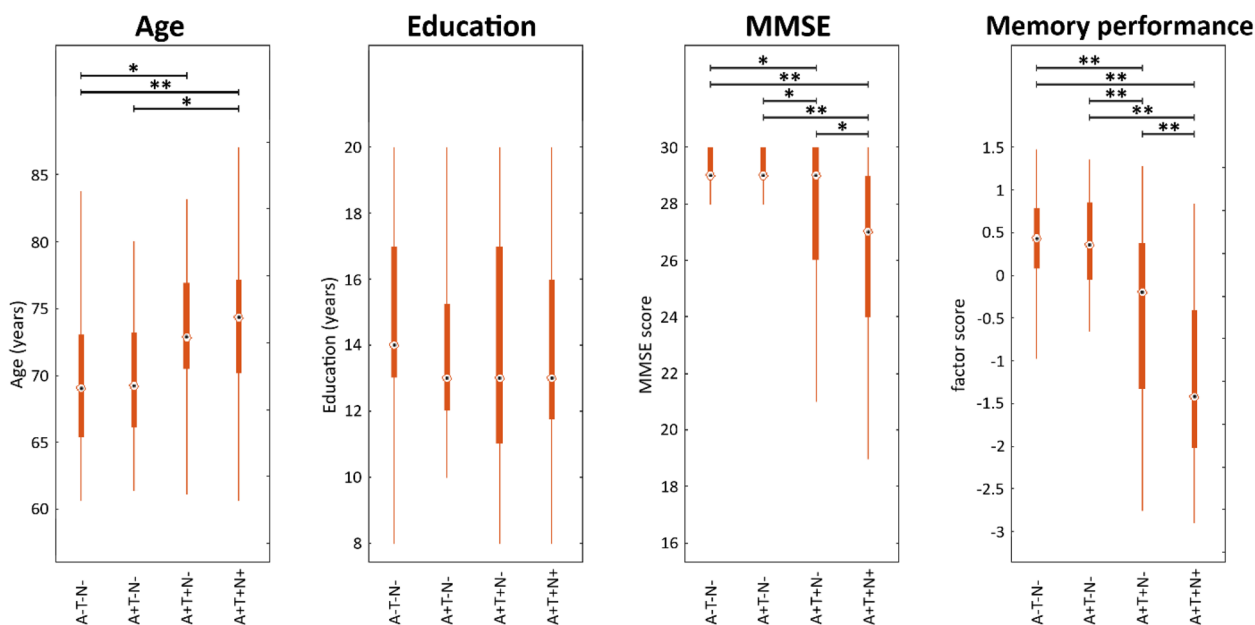
Fig. 2 Comparison between selected ATN groups. Boxplots of age, sex, cognition for selected ATN groups. *: $p < .05$ after Bonferroni correction, **: $p < .001$ after Bonferroni correction

Heinzinger *et al. Alzheimer's Research & Therapy* (2023) 15:50

Page 8 of 18

Fig. 3 Distribution of ATN status and clinical diagnosis. Left: percentual distribution of selected ATN groups per clinical diagnosis; right: percentual distribution of clinical diagnosis per ATN groups

Assessing face validity of the ACH hypothesis using local brain volume

As a next goal, we identified brain regions where volume progression across ATN groups is compatible with the ACH hypothesis. More specifically, if the ACH is true, it might be expected to observe a monotonic decline of volume over groups A−T−N− ➔ A̲+T−N− ➔ A+T̲+N− ➔ A+T+N̲+ in the hippocampal network [25]. The regions showing significant GM volume decline over this ACH sequence (of ATN biomarker conversions) are illustrated in Fig. 4A (log *p* map, *p* < .05 FDR-corrected, N based on hippocampal volume, accounting for covariates age, sex, education, TICV, and WMH). Strongest effects are found in the MTL region (peak: left post. hipp. $x = -28$, $y = -22$, $z = -19$, log $p = 86.70$). Further regions with significant GM volume loss following the ACH sequence are the orbital and basal forebrain, large parts of the temporal lobe, the insular cortex, the basal ganglia, the cingulate gyrus, the precuneus, (medial) premotor regions, and the parietal and occipital lobes. When using CSF total tau instead of hippocampal volume for operationalization of the 'N' category, we observed consistent but slightly less widespread shrinkage of local GM (peak: left ant. hipp. peak $x = -26$, $y = -10$, $z = -17$, log $p = 21.41$, Fig. 4B).

It is important to note that testing for "any" local volume decline over groups that align with the ACH-related

progression might still reveal brain areas where alternative disease progressions are even more likely. Therefore, in an explorative analysis, we compared voxel-wise evidence of the hypothesized ACH progression (or model) against 23 biologically less plausible (permuted) conversion sequences among the ATN classification groups associated with the AD continuum, e.g., the above stated group progression but in reversed order. First, we applied a voxel-based test of monotonic GM volume decline using the Bayesian Information Criterion. Figure 5a illustrates the resulting regions with highest evidence for three selected progressions. Since only one sequence of diagnostic conversions can have the highest evidence in a given brain region (when compared to other progressions), these maps revealed non-overlapping areas of the brain. For 8.99% of all explored GM brain regions, ACH was indeed found to be the most evident progression sequence showing monotonic volume decline (Fig. 5b). This especially involved the anterior MTL, hippocampus, parahippocampal gyrus, and fusiform gyrus while the general pattern of regions most compatible with ACH is similar to the above presented findings.

However, this analysis also suggested that the ACH sequence was not the most evident progression (among 24 tested) in frontal lobe, insular cortex, precentral and postcentral gyri, or the cerebellum. Our analysis revealed several brain regions in which
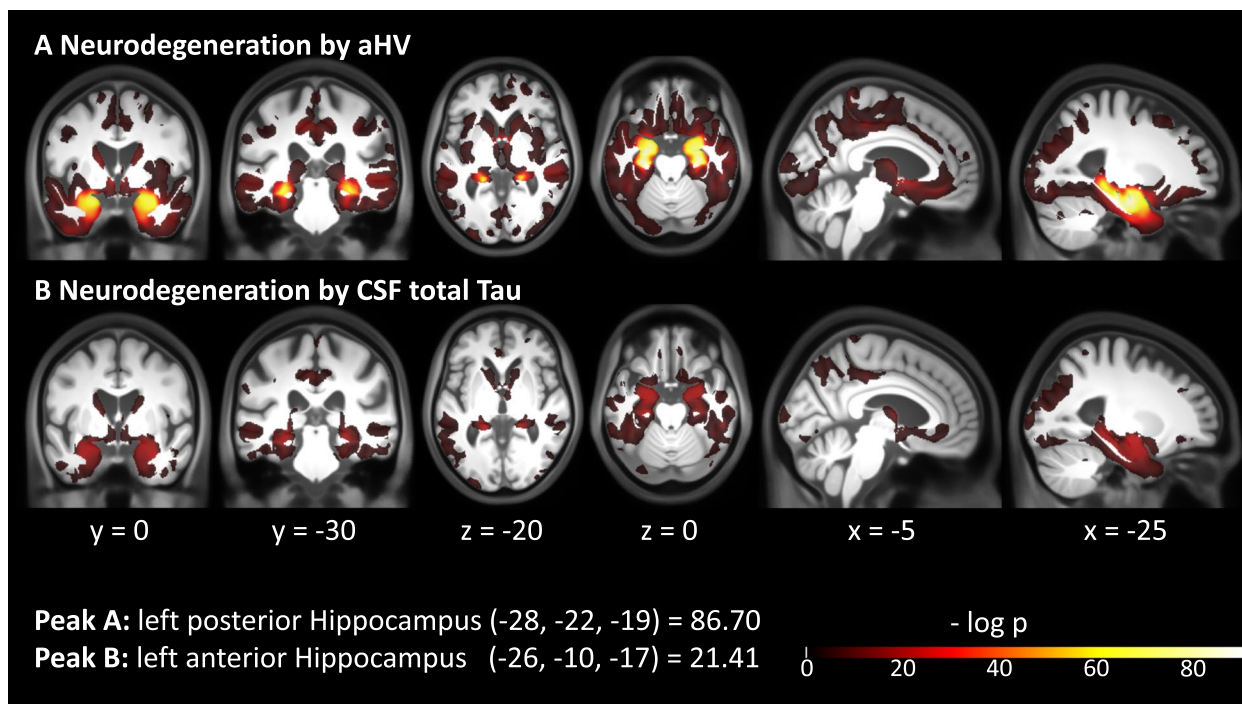
Fig. 4 Volume decline following the ACH sequence. Regions showing significant GM volume loss along the ACH sequence. Unmasked log p map with $p < .05$, FDR-corrected. **A** Neurodegeneration (N) defined by aHV. **B** Neurodegeneration (N) defined by CSF total tau

alternative sequences over ATN groups were better reflective of monotonic volumetric decline. More specifically, alternative progressions AP 1 (A+T−N−➔A+<u>T±</u>N−➔<u>A−T−</u>N−➔A+T+N+) and AP 2 (A+T−N−➔<u>A−</u>T−N−➔<u>A+T±</u>N−➔A+T+<u>N+</u>)

showed highest evidence in 16.28 and 14.05% of the GM respectively (Fig. 5). Interestingly, both assume a transient volume increase when transitioning to amyloid positivity (i.e., GM volume of A+T−N− > A−T−N−) followed by the lowest GM volume in A+T+N+. AP 1
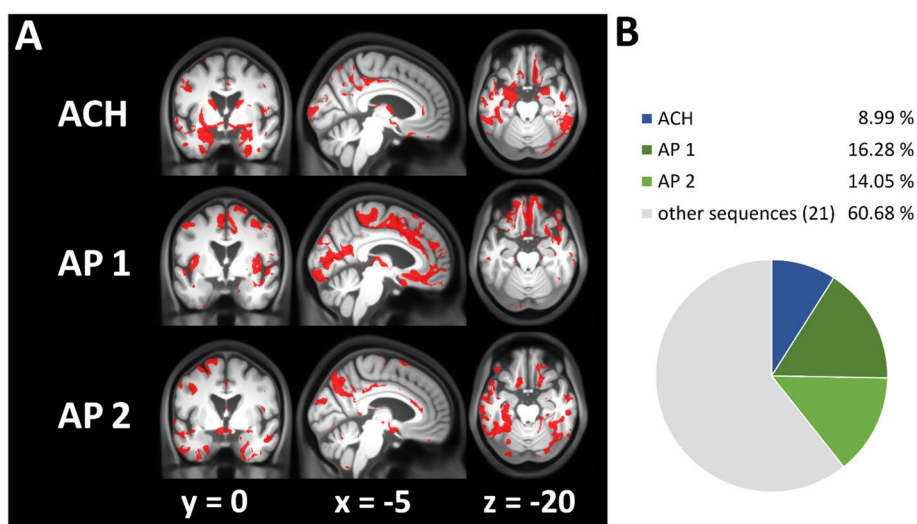
Fig. 5 Face validity of ACH using VBM. Voxel-based evidence for monotonic volume decline over 24 sequences gained by permutation of the ACH sequence (ACH, A−T−N−➔<u>A+</u>T−N−➔A+<u>T±</u>N−➔A+T+<u>N+</u>); AP 1: A+T−N−➔A+<u>T±</u>N−➔<u>A−T−</u>N−➔<u>A+T+N+</u>; AP 2: A+T−N−➔<u>A−</u>T−N−➔<u>A+T±</u>N−➔A+T+<u>N+</u>; **A** voxels where sequence shows highest evidence; **B** percentage of gray matter voxels where sequence has highest evidence

Table 2 Assessment of face validity of the ACH in selected ROIs

Region	Sequence with highest evidence	*T*	*P*	ACH on rank nr. (of 24)	ACH VX%
AMG	ACH	−13.69	2.53e−34	1	80.99
Hippocampus	AP 1	−14.88	6.76e−39	5	26.27
Entorhinal cortex	ACH	−7.30	1.13e−12	1	48.46
Precuneus	AP 2	−3.90	5.76e−05	4	13.78
Braak I/II	ACH	−16.11	1.15e−43	1	25.13
Braak III/IV	Other1	−6.97	8.59e−12	5	17.97
Braak V/VI	Other1	5.06	3.54e−07	5	7.31

ROI-based comparison of evidence for a monotonic volume decline over 24 sequences obtained by permutation of the ACH progression sequence. Braak stage volumes were obtained using aggregated Freesurfer ROI volumes. ACH: A−T−N−➔A+T−N−➔A+T+N−➔A+T+N+; AP 1: A+T−N−➔A+T+N−➔A−T−N−➔A+T+N+; AP 2: A+T−N−➔A−T−N−➔A+T+N−➔A+T+N+; Other1: A+T+N− ➔ A+T−N− ➔ A−T−N− ➔ A+T+N+. ACH VX%: Percentage of voxels with highest evidence for ACH sequence inside the ROI mask

was the conversion sequence having highest evidence in cortical regions (especially frontal lobe, orbital frontal, premotor regions, insular cortex). AP 2 showed highest evidence in parts of the posterior MTL, the middle and posterior cingulate gyrus, and cortical clusters (the precuneus, temporal, parietooccipital lobe).

Table 2 shows the results for a similar but complementary ROI-level analysis of monotonic GM decline in amygdala, hippocampus, entorhinal cortex, and precuneus defined using an MRI atlas. The ACH-based progression was found to be the best fitting sequence to describe monotonic GM volume loss in amygdala and entorhinal cortex. For all ROIs, the ACH progression was found to be among top 5 most likely sequences (out of 24). Surprisingly, AP 1 showed highest evidence for hippocampal ROI volume loss, while the precuneus volume was best described by AP 2. One potential disadvantage of the definition of the "N" category is the dependence on atlas-based ROIs, e.g., for the hippocampus. When using CSF total tau for definition of the "N" category, the ACH sequence was also found to optimally describe monotonic GM loss especially in the MTL. On the ROI level, the ACH sequence was always the most or second most evident pathway (out of 24; Supplemental Files 4 and 5).
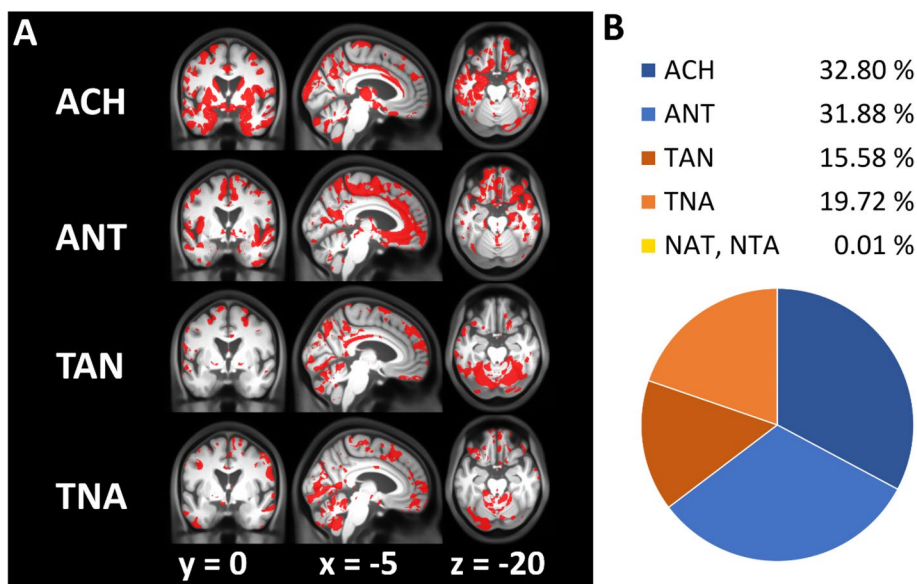
Comparing progression sequences towards AD pathology including non-AD continuum groups

All above comparisons were focused on only four ATN groups from the AD continuum (A−T−N−, A+T−N−, A+T+N−, A+T+N+). However, these AD continuum-related groups do not enable direct comparisons of ACH-implied conversion sequences against an alternative timing of events such as tau positivity preceding amyloid positivity (e.g., A−T+N+ converting to A+T+N+). We therefore compared the ACH-based sequence to five other biologically possible conversion schemes from A−T−N− towards A+T+N+ (denoted as ANT, TAN,

TNA, NAT, NTA). For this comparison, the conversion sequences are denoted in the order of each biomarker becoming positive, e.g., TAN stands for: tau category becomes positive first, amyloid second, neurodegeneration last (A−T−N− ➔ A−T+N− ➔ A+T+N− ➔ A+T+N+). Again, Bayesian Information Criterion (BIC) was used to identify conversion sequences with highest evidence for monotonic volume decline both on a voxel as well as ROI level.

Brain regions with highest evidence for above progressions are characterized in Fig. 6. According to our analysis, A-first sequences (ACH/ATN, ANT), T-first sequences (TAN, TNA), and N-first sequences (NAT, NTA) showed the highest evidence for monotonic volume decline in 64, 35, and 0.01% of GM respectively. Local GM regions with highest likelihood for ACH were especially found in the MTL (with an exception of the right anterior hippocampus and parahippocampal gyrus), but also in the basal ganglia (caudate ncl., putamen, thalamus) and precuneus. More supporting clusters for ACH/ATN were observed in all cortical lobes making it clearly the most likely sequence in large parts of GM in this comparison. The ANT progression showed highest evidence in complementary regions of the MTL not covered by ACH/ATN (see above) with additional regions in the basal ganglia (ncl. accumbens), medial frontal lobe, the insular cortex, and premotor regions. T-first sequences were most likely only in the cerebellum and some cortical regions including the medial occipital lobe. All of these four sequences showed evidence for different parts of the cingulate gyrus. N-first sequences were only seen in very minor portions of the GM.

In the complementary ROI analysis, conversion sequences with monotonic volume decline were compared for same ROIs as above. The most evident sequences for volume loss per ROI and matching effect size are presented in Table 3. Interestingly, ACH/

Fig. 6 Comparing progression sequences towards AD pathology using VBM. Regions with highest evidence for monotonic volume decline assuming 6 potential disease progressions from A−T−N− towards A+T+N+ (ACH, ANT, TAN, TNA, NAT, NTA). Sequences are denoted in the order of biomarker positivity along the pathway (e.g., ANT = amyloid-positivity first, neurodegeneration second, tau last). **A** Voxels where sequence shows highest evidence; Notably, regions of highest evidence for each progression are disjunct. **B** Percentage of gray matter voxels where sequence has highest evidence. N-first sequences (NAT, NTA) are not shown as only few voxels are supported

Table 3 Comparing progression sequences towards AD pathology including non-AD continuum groups in selected ROIs

Region	Best sequence	T	P	ACH on rank nr. (of 6)	ACH VX%
AMG	ACH	−12.93	8.22e−33	1	89.62
Hippocampus	ANT	−18.07	5.74e−55	2	58.18
Entorhinal cortex	ACH	−7.25	9.78e−13	1	89.05
Precuneus	ACH	−3.93	4.86e−05	1	30.92
Braak I/II	ACH	−16.20	1.07e−46	1	57.95
Braak III/IV	ANT	−7.67	5.64e−14	2	46.02
Braak V/VI	ANT	−4.21	1.53e−05	2	28.60

ROI-based comparison of evidence for a monotonic volume decline over 6 possible sequences across ATN groups from A−T−N− towards A+T+N+ (ACH, ANT, TAN, TNA, NAT, NTA). Braak stage volumes are aggregated Freesurfer volumes of regions that mirror Braak stages. *ACH VX%* percentage of voxels with highest evidence for ACH sequence inside the ROI mask

ATN was the most evident progression for amygdala, entorhinal cortex, and precuneus. In the hippocampus however, the ANT progression was found to show the highest evidence for the data. Our analysis revealed no indications for the superiority of T-first or N-first over A-first sequences in these ROIs. Notably, above findings were mainly reproduced using CSF total tau as neurodegeneration marker. Here, ACH was also the most prominent sequence: On the voxel level, more than 41% of GM showed highest evidence for the ACH sequence (Supplemental File 6). On the ROI level, ACH was the most evident sequence with exception of amygdala and entorhinal cortex, where TAN was more likely

which is in contrast to the results of aHV-based neurodegeneration (Supplemental File 7).

Concordance of Braak stage trajectory and the ACH trajectory

In addition to above reported ROIs, the two voxel-based analyses of compatibility of the ACH sequence with monotonic GM volume decline were aggregated for larger Braak stage composite regions (Tables 2 and 3). Here, stage I/II encompasses the hippocampus and entorhinal cortex, stage III/IV the limbic regions, and stage V/VI the remaining cortical regions like precuneus or primary sensory/motor regions. We asked how much of GM at some

stage showed highest evidence for ACH. On the voxel level, the percentage of voxels with highest evidence for the ACH sequence decreased from 25.1% in stage I/II to 7.3% in stage V/VI for the first comparison (face validity of ACH). For the second comparison (including non-AD continuum groups), there was also a noticeable decrease of ACH compatible GM voxels from 58.0% in stage I/II to 28.6% in stage V/VI (see Tables 2 and 3).

Thus, on the ROI level, ACH-related ATN sequence across groups was the most evident conversion sequence which is compatible with a monotonic volume decline in Braak stage I/II. For ROIs reflecting stages III/IV and V/VI, ACH was under the most evident 5 (of 24) respectively 2 (of 6) sequences and thus not the most likely explanation for decline anymore. Test statistics and p values were decreasing with higher Braak stages (stage I/II & III/IV: $p <$ .001; V/VI: $p <$ .05) which supports that ACH compatibility reduces with Braak stage. Using CSF total tau instead of hippocampal volume, a similar trend was observed while more voxels supported ACH in stage I/II (stage I/II & III/IV: $p <$ .001; V/VI: $p >$ .05), Supplemental Files 4 and 7).

Model verification using an ADNI dataset
We verified our ROI analysis comparing model evidence for monotonic volume decline across ATN groups following the ACH progression in a subsample of the ADNI2 dataset. Descriptives of demographic, cognitive, volumetric, and biomarker information can be found in Supplemental File 8. Overall, the validity of our previous ROI-based results could be reproduced using a second and independent dataset (Supplemental Files 9 and 10).

Discussion
Since the ATN classification was postulated in 2016 [24], several studies compared ATN groups to a traditional clinical dementia classification [26, 27, 29, 30, 60–62]. However, a discussion of ATN in context of biological or structural brain changes during AD including local (e.g., voxel-based) brain morphology and the amyloid cascade hypothesis (ACH) can be found to a much lesser extent in previous research [31–33]. This study aimed to focus on these neglected aspects of interest.

Our comparison between ATN status and clinical diagnosis suggested advanced clinical diagnostic status with increasing pathology levels following the ACH group conversion sequence. This is consistent with earlier work [27, 30, 60] where a similar pattern has been observed. The A+T+N+ group has previously been reported to show the highest conversion rate to DAT and an increased risk for cognitive decline [26, 27, 29, 30, 61, 62]. In line with these findings, our results suggested substantial memory performance reductions in later ATN stages.

Using MRI and voxel-based morphometry (VBM), we first tested the face validity of a monotonic GM volume decline over the 4 ATN stages (1) A−T−N− (2) A+T−N− (3) A+T+N− (4) A+T+N+ as implied by the ACH and previous work suggesting GM volume loss during ACH progression in clinical DAT. In contrast to previous with strong prior assumptions about ROIs, our emphasis here was on reporting also complementary voxel-based results. More specifically, in line with previous findings brain regions following monotonic volume decline over ATN stages (1)–(4) involved the hippocampus [17, 45, 46, 63–69], amygdala [17, 45, 46, 63, 66, 68, 69], temporal gyri [17, 46, 65, 67, 68], thalamus [17, 63, 64, 66], precuneus [17, 63, 65, 67], and cingulate gyrus [17, 63–65, 67, 70]. Consistent with some previous work [64, 67, 70], a decline in parts of the cingulate gyrus and insula were observed in our study. Regions that are expected to be affected in very late AD such as frontal [17, 67] and occipital [45, 64, 65, 67] lobes or less affected such as those around central sulcus [46, 65, 67] showed only minor effects in terms of a monotonic decline over ATN stages (1)–(4).

Notably, the ACH is still part of an ongoing discussion as anti-amyloid treatments showed only limited success [71, 72]. Furthermore, the causal link between amyloid, tau, and resulting neurodegeneration and dementia is a challenging research topic [19, 20] which might be mediated by alterations in neuropil [71], synapses [73], or functional connectivity [74]. A further influence on the cognitive performance in AD may be caused by the breakdown of the blood-brain barrier as indicated by Nation et al. [75]. The authors pointed out that this effect is independent of CSF Aβ or tau level changes and shows a distribution pattern which is generally compatible with the progress of the Braak stages and our findings. The breakdown of the blood-brain barrier further may impact the glymphatic transport and thereby the elimination of Aβ and tau from neuronal tissue over the CSF towards extracranial spaces [76] and finally may alternate ATN group assignments when measured using CSF samples.

Our study revealed strong evidence for an ACH-related monotonic atrophy pattern both on the voxel level but also on ROI level especially focussed on typical AD-related regions such as the MTL. However, we also observed many gray matter areas where a monotonic volume trajectory along the ACH-implied group progression sequence did show the highest evidence. We identified alternative progressions (denoted AP 1 and AP 2) indicating that there are several cortical regions where the GM volume was found to be higher in the A+T−N− group than in A−T−N−. These were mainly found in cortical regions which are often less strongly affected by AD [17, 67]. One might speculate that either

amyloid deposition-related tissue expansion [77, 78] and/or sampling effects due to individual differences of brain reserve [79] might alter brain volume patterns across ATN groups and the progression along the ACH trajectory. A biphasic model of neurodegeneration has been previously suggested by Fortea et al. [77] hypothesizing that cortical thickening might occur when Aβ becomes abnormal, which presumably reflects inflammation-related swelling, followed by thinning once tau pathology emerges. The authors found amyloid-related thickness increases in middle temporal, inferior and superior parietal, occipital regions and precuneus which is similar to our findings. Another recent publication also observed amyloid-related regional volume increase in A+T−N− for the basal forebrain, postcentral gyrus, middle occipital gyrus, and putamen when comparing to A−T−N− [80]. As described above, large parts of the cingulate gyrus did suggest a monotonic volume decline along ACH group progression. However, ACH did not necessarily reveal the highest evidence in the entire cingulate as there were also portions with highest evidence for non-monotonic volume decline (subcallosal to middle cingulate in AP1 and middle to posterior cingulate in AP2). This renders the cingulate a potential candidate region for brain reserve or biphasic model that requires further research.

Under the assumption that patients will convert from negative to positive ATN biomarkers, six patterns of conversions are possible when non-AD pathology ATN groups are additionally included. When testing for monotonic volume decline across these patterns, the highest evidence was found for sequences where amyloid converts before either tau or neurodegeneration (e.g., ATN, ANT), and this was observed in 65% of all gray matter brain areas, especially in AD-related regions. We were able to replicate our finding using ROI-based analyses. In contrast, conversion patterns where tau converted before amyloid (TAN, TNA) showed highest evidence for a monotonic volume decline in cortical regions that are atypical for AD pathology. Support for our findings comes from a longitudinal study of 262 non-demented elderly to monitor ATN biomarker progress [32]. It was found that ACH was the most common path of biomarker conversion, but also ANT, TAN, and NAT occurred. In contrast, we observed no evidence for NAT in terms of GM volume decreases. It is worth mentioning that per definition, A−T+ or A−N+ groups are not part of the AD continuum, these groups might initially point to other diseases like primary tauopathies, hippocampal sclerosis/TDP-43, or ischaemic diseases [24]. As remarked by [1] and [32], the occurrence of conversion sequences other than ACH in real-world data might be explained by (a) coincidence of AD- and non-AD

pathologic changes (e.g., in A+T−N+) or (b) long-time subthreshold biomarker trends matching the ACH that are not recognized due to a binary classification with disadvantageous thresholds [1, 32]. Another study provides more support for our hypothesis of an ACH-related temporal order of biomarker progress by monitoring between-group biomarker changes in an longitudinal approach using the ATN classification [31]. A related approach for ordering pathological events during Alzheimer's disease cascade using different model assumptions is the event-based modelling [81, 82]. The authors predicted a continuous pathological sequence using a maximum likelihood estimation to reduce variance and errors without having defined *a priori* biomarker cutoffs. As the authors described, this comes with the limitation that events are assumed to be independent of each other. Their findings offered support for the ACH, while they also found limited evidence for tau pathology-first, amyloid-second on the CSF level. Future studies might focus on comparisons across different approaches.

Furthermore, our morphometric study revealed evidence to support the consistency between the ACH and Braak staging. Brain regions that are expected to be earlier affected by AD pathology-linked tau deposition (stage I-IV, MTL, limbic system) showed stronger evidence for monotonic GM volume decline over a sequence of conversions than later stages (stage V/VI, cortical regions). As it is already known that brain atrophy often follows tau and NFT aggregation [66], both hypotheses were not mutually exclusive. In our analysis, the stronger evidence for volume decline in the amygdala was surprising when comparing to the hippocampus. As [83] remarked, tau pathology in the amygdala is already beginning with Braak stage I/II. However, this effect was not reproducible with neurodegeneration by CSF total tau.

It is known that alternative choices of markers for the N category may have a strong impact on ATN status assignment and longitudinal prediction of cognition [84, 85]. The large pool of possible classification methods limits intercomparability between ATN studies dramatically. In our large study, both variants of ATN classification approaches showed converging evidence for the ACH hypothesis. We were not able to determine a superior combination, as both tested N markers have advantages and caveats. The usage of aHV leads to overall stronger effect sizes but one might argue that there is a circularity in defining ATN groups using volumetry and analyzing ATN-related local brain morphometry. Neurodegeneration defined by aHV is a discrete marker of general neuronal loss and the group assignment was carried out using a ROI-rather than voxel-based approach. GM volume (as analyzed by VBM) on the other hand allows a

continuous whole brain local analysis on the voxel level and does not align with N for most brain regions.

Although VBM revealed the highest evidence for ACH-related monotonic volume decline in the hippocampus, regions in cortical areas showed compatible monotonic progressions. Taking advantage of the voxel-based approach, differences between sequences could be identified even inside the hippocampus (ACH supports anterior hippocampus, AP2 posterior hippocampus). It is worth mentioning that the approach is not limited to VBM measurements; in contrast to developmental and plasticity studies, stronger expectations for monotonic trajectories do exist for brain volumes in aging and AD. Alternative N categories (such as CSF total tau) might also have limitations. The combination of CSF phospho-tau (T category) and CSF total tau (N category) is used in some studies [26, 61, 62], while a strong correlation between both markers strongly underrepresents some ATN groups (A?T+N−, A?T−N+). In a recent publication [28], it was possible to replace CSF total tau by CSF phospho-tau without significant impact on the model. Although there is only a weak correlation between aHV and CSF total tau as N markers in our study, a similar pattern of local GM volume decline was revealed. This further suggests that a morphometrical analysis with aHV is applicable.

Our results were coarsely supported by a replication analysis using an independent ADNI sample with similar features including CSF Aβ42 instead of the Aβ42over40 ratio and Freesurfer 5.1 instead of Version 6.0.

Limitations

This study has several methodological limitations. The first challenge was the hippocampal cutoff estimation: The large sample size does not allow to perform atrophy reference methods like autopsy or visual rating of FDG-PET or MRI. Thus, no estimation of sensitivity or specificity was possible, which prohibits a ROC analysis and Youden's index. Although aHV has a clear unimodal Gaussian distribution, it is possible to perform a Gaussian mixture modelling to separate between normal and decreased volumes. A similar approach was performed by [80]. As our data is cross-sectional, no real progression over disease progression and conversions can be modelled and tested. We compensated potential influences of covariates by correcting for demographic marker such as age, sex, and education, vascular damage, and intracranial volume. This improves comparability (matching) across different ATN groups and increases validity of the underlying cross-sectional progression. Once available, longitudinal DELCODE follow-up data will be used for further validation.

Conclusion

Early amyloid status conversion (before tau and neurodegeneration) aligns with pattern of brain volume loss observed during AD progression. The ATN classification and the amyloid cascade hypothesis are compatible with a monotonic progression of MTL atrophy, but using the ATN classification system for staging our study revealed indications for non-monotonic progressions in other areas such as several cortical fields.

Abbreviations

ACH	Amyloid cascade hypothesis
AD	Alzheimer's disease
ADNI	Alzheimer's Disease Neuroimaging Initiative
DAT	Dementia of Alzheimer's type
aHV	Adjusted hippocampal volume
AN(C)OVA	Analysis of (co-) variance
ATN	Classification based on amyloid / tau / neurodegeneration pathology
BIC	Bayesian Information Criterion
CAT	Computational Anatomy Toolbox
CDR	Clinical Dementia Rating
CERAD	Consortium to Establish a Registry for Alzheimer's Disease
NC	Noncomplaining healthy control
CSF	Cerebrospinal fluid
FDR	False discovery rate
FLAIR	Fluid attenuated inversion recovery
GM	Gray matter
GMM	Gaussian mixture modelling
MCI	Mild cognitive impairment
MMSE	Mini-Mental State Examination
MPRAGE	Magnetization prepared rapid gradient echo
MRI	Magnetic resonance imaging
MTL	Medial temporal lobe
NFT	Neurofibrillary tangles
ROI	Region of interest
SCD	Subjective cognitive decline
SPM	Statistical parametric mapping
TICV	Total intracranial volume
VBM	Voxel-based morphometry
WM	White matter
WMH	White matter hyperintensities

Supplementary Information

The online version contains supplementary material available at https://doi.org/10.1186/s13195-023-01185-x.

Additional file 1. The impact of Gaussian blurring with different FWHM kernels sizes on model evidence for ACH. Displayed is one slice (y = 0) for each FWHM kernel size. Shown is the voxel-based evidence for monotonic volume decline of the ACH sequence (➡ A+T-N- ➡ A+T+N- ➡ A+T+N+) over 24 sequences obtained by permutation. For our model, we selected the 6 mm FWHM kernel as a compromise between reducing noise and preserving local information of volume differences. Red: voxels where sequence shows highest evidence. Neurodegeneration (N) by aHV.

Additional file 2. Comparison between selected ATN groups using CSF-total-Tau. Boxplots of age, sex, cognition for selected ATN groups. *: p < .05 after Bonferroni correction, **: p < .001 after Bonferroni correction. Neurodegeneration (N) by CSF Total Tau.

Additional file 3. Distribution of ATN status and clinical diagnosis using CSF-total-Tau. Left: percentual distribution of selected ATN groups per clinical diagnosis; right: percentual distribution of clinical diagnosis per ATN groups. Neurodegeneration (N) by CSF Total Tau.

Heinzinger *et al. Alzheimer's Research & Therapy*   (2023) 15:50

Page 15 of 18

Additional file 4. Assessment of face validity of the ACH using selected ROIs and CSF-total-Tau. ROI based comparison of evidence for a monotonic volume decline over 24 sequences obtained by permutation of the ACH progression sequence. Braak stage volumes were obtained using aggregated Freesurfer ROI volumes. Other2: A-T-N- ➔ A+T+N- ➔ A+T-N- ➔ A+T+N+; Other3: A+T-N- ➔ A-T-N- ➔ A+T+N- ➔ A+T+N+. ACH VX%: Percentage of voxels with highest evidence for ACH sequence inside the ROI mask. Neurodegeneration (N) by CSF Total Tau.

Additional file 5. Face validity of ACH using VBM and CSF-total-Tau. Voxel-based evidence for monotonic volume decline over 24 sequences gained by permutation of the ACH sequence (ACH, A-T-N-➔A+T-N-➔A+T+N-➔A+T+N+); AP 1: A+T-N-➔A+T+N-➔A-T-N-➔A+T+N+; AP 2: A+T-N-➔A-T-N-➔A+T+N-➔A+T+N+; A: voxels where sequence shows highest evidence; B: percentage of gray matter voxels where sequence has highest evidence. Neurodegeneration (N) by CSF Total Tau.

Additional file 6. Comparing progression sequences towards AD pathology using VBM and CSF-total-Tau. Voxel-based evidence for monotonic volume decline over 6 possible sequences from A-T-N- towards A+T+N+ (ACH, ANT, TAN, TNA, NAT, NTA). Sequences are denoted in the order of biomarker positivity along the pathway (e.g. ANT = Amyloid-positivity first, Neurodegeneration second, Tau last). A: voxels where sequence shows highest evidence; B: percentage of gray matter voxels where sequence has highest evidence. N-first sequences (NAT, NTA) are not shown as only few voxels are supported. Neurodegeneration (N) by CSF Total Tau.

Additional file 7. Comparing progression sequences towards AD pathology using selected ROIs and CSF-total-Tau. ROI based comparison of evidence for a monotonic volume decline over 6 possible sequences across ATN groups from A-T-N- towards A+T+N+ (ACH, ANT, TAN, TNA, NAT, NTA) including also non-AD continuum groups. Braak stage volumes are aggregated Freesurfer ROI volumes. ACH VX%: Percentage of voxels with highest evidence for ACH sequence inside the ROI mask. Neurodegeneration (N) by CSF Total Tau.

Additional file 8. ADNI2 sample characteristics and ATN group classification. Overview of descriptive characteristics of the ADNI2 sample and its ATN groups used for out-of sample replication. Non-AD pathologic change: ATN groups that are related to neuronal conditions other than AD; Alzheimer's continuum groups: Aβ-positive groups that are related to AD; aHV: adjusted hippocampal volume; WMH: white matter hyperintensities.

Additional file 9. Assessment of face validity of the ACH using selected ROIs in the ADNI2 subsample. ROI based comparison of the evidence for a for monotonic volume decline over 24 sequences obtained by permutation of the ACH progression sequence. Braak stage volumes were obtained using aggregated Freesurfer ROI volumes. AP 1: A+T-N-➔A+T+N-➔A-T-N-➔A+T+N+; AP 2: A+T-N-➔A-T-N-➔A+T+N-➔A+T+N+; Other2: A-T-N- ➔ A+T+N- ➔ A+T-N- ➔ A+T+N+; Other4: A-T-N- ➔ A+T+N+ ➔ A+T+N- ➔ A+T-N-. Neurodegeneration (N) by aHV.

Additional file 10. Comparing progression sequences towards AD pathology using selected ROIs and ADNI2. ROI based comparison of evidence for a monotonic volume decline over 6 possible sequences across ATN groups from A-T-N- towards A+T+N+ (ACH, ANT, TAN, TNA, NAT, NTA) including also non-AD continuum groups. Braak stage volumes are aggregated Freesurfer ROI volumes. Neurodegeneration (N) by aHV.

Availability of data and materials
The code used during the current study is available from the corresponding author on reasonable request. DELCODE data, study protocol, and biomaterials can be shared with partners based on individual data and biomaterial transfer agreements. Requests can be addressed to the DELCODE steering committee. The ADNI database can be accessed at: https://adni.loni.usc.edu/

Declarations

Ethics approval and consent to participate
DELCODE is retrospectively registered at the German Clinical Trials Register (DRKS00007966), (04/05/2015) and was approved by the ethical committees of the medical faculties of all participating sites: the ethical committees of Berlin (Charite, University Medicine), Bonn, Cologne, Goettingen, Magdeburg, Munich (Ludwig-Maximilians-University), Rostock, and Tuebingen. The process was led and coordinated by the ethical committee of the medical faculty of the University of Bonn. All committees gave ethical approval for this work. All participants gave written informed consent to participate. DELCODE was conducted in accordance with the Declaration of Helsinki.
ADNI was approved by the institutional review boards of all participating centres: Oregon Health & Science University; University of Southern California; University of California – San Diego; University of Michigan; Mayo Clinic, Rochester; Baylor College of Medicine; Columbia University Medical Center; Washington University, St. Louis; University of Alabama – Birmingham; Mount Sinai School of Medicine; Rush University Medical Center; Wien Center; Johns Hopkins University; University of South Florida: USF Health Byrd Alzheimer's Institute; New York University; Duke University Medical Center; University of Pennsylvania; University of Kentucky; University of Pittsburgh; University of Rochester Medical Center; University of California Irvine IMIND; University of Texas Southwestern Medical School; Emory University; University of Kansas, Medical Center; University of California, Los Angeles; Mayo Clinic, Jacksonville; Indiana University; Yale University School of Medicine; McGill Univ., Montreal-Jewish General Hospital; Sunnybrook Health Sciences, Ontario; U.B.C. Clinic for AD & Related Disorders; St. Joseph's Health Care; Northwestern University; Nathan Kline Institute; University of California, San Francisco; Georgetown University Medical Center; Brigham and Women's Hospital;

Stanford University; Banner Sun Health Research Institute; Boston University; Howard University; Case Western Reserve University; University of California, Davis – Sacramento; Dent Neurologic Institute; Parkwood Institute; University of Wisconsin; Banner Alzheimer's Institute; Ohio State University; Albany Medical College; University of Iowa College of Medicine; Wake Forest University Health Sciences; Rhode Island Hospital; Cleveland Clinic Lou Ruvo Center for Brain Health; Roper St. Francis Healthcare; Houston Methodist Neurological Institute; Barrow Neurological Institute; Vanderbilt University Medical Center; Long Beach VA Neuropsychiatric Research Program; Butler Hospital Memory and Aging Program; Neurological Care of CNY; Hartford Hospital, Olin Neuropsychiatry Research Center; Dartmouth-Hitchcock Medical Center; Cornell University. All participants or their authorized representatives gave written informed consent to participate. ADNI was conducted in accordance with the Declaration of Helsinki.

Consent for publication
Not applicable.

Competing interests
The authors declare that they have no competing interests.

Author details
[1]German Center for Neurodegenerative Diseases (DZNE), Magdeburg, Germany. [2]Institute of Cognitive Neurology and Dementia Research (IKND), University Hospital Magdeburg, Otto-von-Guericke University, Leipziger Str. 44, 39120 Magdeburg, Germany. [3]German Center for Neurodegenerative Diseases (DZNE), Berlin, Germany. [4]Department of Psychiatry, Charité-Universitätsmedizin Berlin, Campus Benjamin Franklin, Berlin, Germany. [5]Center for Stroke Research Berlin, Charité-Universitätsmedizin, Berlin, Germany. [6]Department of Psychiatry and Psychotherapy, Charité, Berlin, Germany. [7]Department of Psychiatry and Psychotherapy, School of Medicine, Technical University of Munich, Munich, Germany. [8]University of Edinburgh and UK DRI, Edinburgh, UK. [9]German Center for Neurodegenerative Diseases (DZNE), Bonn, Germany. [10]Department of Neurodegenerative Diseases and Geriatric Psychiatry/Psychiatry, University of Bonn Medical Center, Bonn, Germany. [11]German Center for Neurodegenerative Diseases (DZNE), Göttingen, Germany. [12]Department of Psychiatry and Psychotherapy, University Medical Center Göttingen, University of Göttingen, Göttingen, Germany. [13]Department of Medical Sciences, Neurosciences and Signaling Group, Institute of Biomedicine (iBiMED), University of Aveiro, Aveiro, Portugal. [14]Department of Psychiatry, Medical Faculty, University of Cologne, Cologne, Germany. [15]Excellence Cluster on Cellular Stress Responses in Aging-Associated Diseases (CECAD), University of Cologne, Cologne, Germany. [16]German Center for Neurodegenerative Diseases (DZNE), Munich, Germany. [17]Institute for Stroke and Dementia Research (ISD), University Hospital, LMU Munich, Munich, Germany. [18]Department of Psychiatry and Psychotherapy, University Hospital, LMU Munich, Munich, Germany. [19]Munich Cluster for Systems Neurology (SyNergy), Munich, Germany. [20]Ageing Epidemiology Research Unit (AGE), School of Public Health, Imperial College London, London, UK. [21]German Center for Neurodegenerative Diseases (DZNE), Rostock, Germany. [22]Department of Psychosomatic Medicine, Rostock University Medical Center, Rostock, Germany. [23]German Center for Neurodegenerative Diseases (DZNE), Tübingen, Germany. [24]Section for Dementia Research, Hertie Institute for Clinical Brain Research and Department of Psychiatry and Psychotherapy, University of Tübingen, Tübingen, Germany. [25]Department of Neurology, University of Bonn, Bonn, Germany. [26]MR-Research in Neurosciences, Department of Cognitive Neurology, Georg-August-University Göttingen, Göttingen, Germany. [27]Bernstein Center for Computational Neuroscience, Charité-Universitätsmedizin, Berlin, Germany. [28]Department for Biomedical Magnetic Resonance, University of Tübingen, Tübingen, Germany. [29]Institute for Medical Biometry, University Hospital Bonn, Bonn, Germany.

References
1. Jack CR, Knopman DS, Jagust WJ, et al. Tracking pathophysiological processes in Alzheimer's disease: an updated hypothetical model of dynamic biomarkers. Lancet Neurol. 2013;12(2):207–16. https://doi.org/10.1016/S1474-4422(12)70291-0.
2. Villemagne VL, Burnham S, Bourgeat P, et al. Amyloid β deposition, neurodegeneration, and cognitive decline in sporadic Alzheimer's disease: a prospective cohort study. Lancet Neurol. 2013;12(4):357–67. https://doi.org/10.1016/S1474-4422(13)70044-9.
3. Dean DC, Jerskey BA, Chen K, et al. Brain differences in infants at differential genetic risk for late-onset Alzheimer disease: a cross-sectional imaging study. JAMA Neurol. 2014;71(1):11–22. https://doi.org/10.1001/jamaneurol.2013.4544.
4. Thal DR, Capetillo-Zarate E, Del Tredici K, Braak H. The development of amyloid beta protein deposits in the aged brain. Sci Aging Knowl Environ. 2006;2006(6):re1. https://doi.org/10.1126/sageke.2006.6.re1.
5. Braak H, Braak E. Neuropathological stageing of Alzheimer-related changes. Acta Neuropathol. 1991;82(4):239–59. https://doi.org/10.1007/bf00308809.
6. Janelidze S, Zetterberg H, Mattsson N, et al. CSF Aβ42/Aβ40 and Aβ42/Aβ38 ratios: better diagnostic markers of Alzheimer disease. Ann Clin Transl Neurol. 2016;3(3):154–65. https://doi.org/10.1002/acn3.274.
7. Ritchie C, Smailagic N, Noel-Storr AH, Ukoumunne O, Ladds EC, Martin S. CSF tau and the CSF tau/ABeta ratio for the diagnosis of Alzheimer's disease dementia and other dementias in people with mild cognitive impairment (MCI). Cochrane Database Syst Rev. 2017;3:CD010803. https://doi.org/10.1002/14651858.CD010803.pub2.
8. Blennow K, Hampel H. CSF markers for incipient Alzheimer's disease. Lancet Neurol. 2003;2(10):605–13. https://doi.org/10.1016/s1474-4422(03)00530-1.
9. Hampel H, Bürger K, Teipel SJ, Bokde ALW, Zetterberg H, Blennow K. Core candidate neurochemical and imaging biomarkers of Alzheimer's disease. Alzheimers Dement. 2008;4(1):38–48. https://doi.org/10.1016/j.jalz.2007.08.006.
10. Nathan PJ, Lim YY, Abbott R, et al. Association between CSF biomarkers, hippocampal volume and cognitive function in patients with amnestic mild cognitive impairment (MCI). Neurobiol Aging. 2017;53:1–10. https://doi.org/10.1016/j.neurobiolaging.2017.01.013.
11. Selkoe DJ. The molecular pathology of Alzheimer's disease. Neuron. 1991;6(4):487–98. https://doi.org/10.1016/0896-6273(91)90052-2.
12. Hardy JA, Higgins GA. Alzheimer's disease: the amyloid cascade hypothesis. Science. 1992;256(5054):184–5. https://doi.org/10.1126/science.1566067.
13. Reitz C. Alzheimer's disease and the amyloid cascade hypothesis: a critical review. Int J Alzheimers Dis. 2012;2012:369808. https://doi.org/10.1155/2012/369808.
14. Hou Y, Dan X, Babbar M, et al. Ageing as a risk factor for neurodegenerative disease. Nat Rev Neurol. 2019;15(10):565–81. https://doi.org/10.1038/s41582-019-0244-7.
15. Yamazaki Y, Zhao N, Caulfield TR, Liu C-C, Bu G. Apolipoprotein E and Alzheimer disease: pathobiology and targeting strategies. Nat Rev Neurol. 2019;15(9):501–18. https://doi.org/10.1038/s41582-019-0228-7.
16. Prins ND, Scheltens P. White matter hyperintensities, cognitive impairment and dementia: an update. Nat Rev Neurol. 2015;11(3):157–65. https://doi.org/10.1038/nrneurol.2015.10.
17. Yang J, Pan P, Song W, et al. Voxelwise meta-analysis of gray matter anomalies in Alzheimer's disease and mild cognitive impairment using anatomic likelihood estimation. J Neurol Sci. 2012;316(1-2):21–9. https://doi.org/10.1016/j.jns.2012.02.010.
18. Matsuda H. Voxel-based Morphometry of Brain MRI in normal aging and Alzheimer's disease. Aging Dis. 2013;4(1):29–37 https://www.ncbi.nlm.nih.gov/pmc/articles/PMC3570139/ Accessed 2 Dec 2020.
19. Armstrong RA. A critical analysis of the 'amyloid cascade hypothesis'. Folia Neuropathol. 2014;3:211–25. https://doi.org/10.5114/fn.2014.45562.
20. Busche MA, Hyman BT. Synergy between amyloid-β and tau in Alzheimer's disease. Nat Neurosci. 2020;23(10):1183–93. https://doi.org/10.1038/s41593-020-0687-6.
21. Schöll M, Lockhart SN, Schonhaut DR, et al. PET imaging of tau deposition in the aging human brain. Neuron. 2016;89(5):971–82. https://doi.org/10.1016/j.neuron.2016.01.028.
22. Maass A, Landau S, Baker SL, et al. Comparison of multiple tau-PET measures as biomarkers in aging and Alzheimer's disease. Neuroimage. 2017;157:448–63. https://doi.org/10.1016/j.neuroimage.2017.05.058.
23. Matsuda H. MRI morphometry in Alzheimer's disease. Ageing Res Rev. 2016;30:17–24. https://doi.org/10.1016/j.arr.2016.01.003.
24. Jack CR, Bennett DA, Blennow K, et al. A/T/N: An unbiased descriptive classification scheme for Alzheimer disease biomarkers. Neurology. 2016;87(5):539–47. https://doi.org/10.1212/WNL.0000000000002923.

Heinzinger *et al. Alzheimer's Research & Therapy*   (2023) 15:50

Page 17 of 18

25. Jack CR, Bennett DA, Blennow K, et al. NIA-AA research framework: toward a biological definition of Alzheimer's disease. Alzheimers Dement. 2018;14(4):535–62. https://doi.org/10.1016/j.jalz.2018.02.018.

26. Soldan A, Pettigrew C, Fagan AM, et al. ATN profiles among cognitively normal individuals and longitudinal cognitive outcomes. Neurology. 2019;92(14):e1567–79. https://doi.org/10.1212/WNL.0000000000007248.

27. Altomare D, de Wilde A, Ossenkoppele R, et al. Applying the ATN scheme in a memory clinic population: the ABIDE project. Neurology. 2019;93(17):e1635–46. https://doi.org/10.1212/WNL.0000000000008361.

28. van Maurik IS, Vos SJ, Bos I, et al. Biomarker-based prognosis for people with mild cognitive impairment (ABIDE): a modelling study. Lancet Neurol. 2019;18(11):1034–44. https://doi.org/10.1016/S1474-4422(19)30283-2.

29. Jack CR, Wiste HJ, Therneau TM, et al. Associations of amyloid, tau, and neurodegeneration biomarker profiles with rates of memory decline among individuals without dementia. JAMA. 2019;321(23):2316–25. https://doi.org/10.1001/jama.2019.7437.

30. Yu J-T, Li J-Q, Suckling J, et al. Frequency and longitudinal clinical outcomes of Alzheimer's AT(N) biomarker profiles: a longitudinal study. Alzheimers Dement. 2019;15(9):1208–17. https://doi.org/10.1016/j.jalz.2019.05.006.

31. Guo T, Korman D, Baker SL, Landau SM, Jagust WJ. Longitudinal cognitive and biomarker measurements support a unidirectional pathway in Alzheimer's disease pathophysiology. Biol Psychiatry. 2020. https://doi.org/10.1016/j.biopsych.2020.06.029.

32. Tan M-S, Ji X, Li J-Q, et al. Longitudinal trajectories of Alzheimer's ATN biomarkers in elderly persons without dementia. Alzheimers Res Ther. 2020;12(1):55. https://doi.org/10.1186/s13195-020-00621-6.

33. Ekman U, Ferreira D, Westman E. The A/T/N biomarker scheme and patterns of brain atrophy assessed in mild cognitive impairment. Sci Rep. 2018;8(1):8431. https://doi.org/10.1038/s41598-018-26151-8.

34. Jessen F, Spottke A, Boecker H, et al. Design and first baseline data of the DZNE multicenter observational study on predementia Alzheimer's disease (DELCODE). Alzheimers Res Ther. 2018;10(1):15. https://doi.org/10.1186/s13195-017-0314-2.

35. McKhann G, Drachman D, Folstein M, Katzman R, Price D, Stadlan EM. Clinical diagnosis of Alzheimer's disease: report of the NINCDS-ADRDA Work Group under the auspices of Department of Health and Human Services Task Force on Alzheimer's Disease. Neurology. 1984;34(7):939–44. https://doi.org/10.1212/wnl.34.7.939.

36. Folstein MF, Folstein SE, McHugh PR. Mini-mental state: a practical method for grading the state of patients for the clinician. J Psychiatr Res. 1975;12(3):189–98. https://doi.org/10.1016/0022-3956(75)90026-6.

37. Wolfsgruber S, Kleineidam L, Guski J, et al. Minor neuropsychological deficits in patients with subjective cognitive decline. Neurology. 2020;95(9):e1134–43. https://doi.org/10.1212/WNL.0000000000010142.

38. Wellcome Trust Centre for Human Neuroimaging, University College London. Statistical Parametric Mapping software https://www.fil.ion.ucl.ac.uk/spm/. Accessed 8 Feb 2022.

39. Structural Brain Mapping group, Jena University Hospital. CAT-Toolbox http://www.neuro.uni-jena.de/cat/. Accessed 8 Feb 2022.

40. Rajapakse JC, Giedd JN, Rapoport JL. Statistical approach to segmentation of single-channel cerebral MR images. IEEE Trans Med Imaging. 1997;16(2):176–86. https://doi.org/10.1109/42.563663.

41. Ashburner J, Friston KJ. Diffeomorphic registration using geodesic shooting and Gauss-Newton optimisation. Neuroimage. 2011;55(3):954–67. https://doi.org/10.1016/j.neuroimage.2010.12.049.

42. Laboratory for Computational Neuroimaging, Massachusetts General Hospital. Freesurfer. http://surfer.nmr.mgh.harvard.edu/. Accessed 8 Feb 2022.

43. Fischl B, van der Kouwe A, Destrieux C, et al. Automatically parcellating the human cerebral cortex. Cereb Cortex. 2004;14(1):11–22. https://doi.org/10.1093/cercor/bhg087.

44. Fischl B, Salat DH, Busa E, et al. Whole brain segmentation. Neuron. 2002;33(3):341–55. https://doi.org/10.1016/s0896-6273(02)00569-x.

45. Busatto GF, Diniz BS, Zanetti MV. Voxel-based morphometry in Alzheimer's disease. Expert Rev Neurother. 2008;8(11):1691–702. https://doi.org/10.1586/14737175.8.11.1691.

46. Ferreira LK, Diniz BS, Forlenza OV, Busatto GF, Zanetti MV. Neurostructural predictors of Alzheimer's disease: a meta-analysis of VBM studies. Neurobiol Aging. 2011;32(10):1733–41. https://doi.org/10.1016/j.neurobiolaging.2009.11.008.

47. Leandrou S, Petroudi S, Kyriacou PA, Reyes-Aldasoro CC, Pattichis CS. Quantitative MRI brain studies in mild cognitive impairment and Alzheimer's disease: a methodological review. IEEE Rev Biomed Eng. 2018;11:97–111. https://doi.org/10.1109/RBME.2018.2796598.

48. Teipel SJ, Meindl T, Grinberg L, Heinsen H, Hampel H. Novel MRI techniques in the assessment of dementia. Eur J Nucl Med Mol Imaging. 2008;35(Suppl 1):S58–69. https://doi.org/10.1007/s00259-007-0703-z.

49. Baker SL, Maass A, Jagust WJ. Considerations and code for partial volume correcting 18F-AV-1451 tau PET data. Data Brief. 2017;15:648–57. https://doi.org/10.1016/j.dib.2017.10.024.

50. Iglesias JE, Augustinack JC, Nguyen K, et al. A computational atlas of the hippocampal formation using ex vivo, ultra-high resolution MRI: application to adaptive segmentation of in vivo MRI. Neuroimage. 2015;115:117–37. https://doi.org/10.1016/j.neuroimage.2015.04.042.

51. Koncz R, Sachdev PS. Are the brain's vascular and Alzheimer pathologies additive or interactive? Curr Opin Psychiatry. 2018;31(2):147–52. https://doi.org/10.1097/YCO.0000000000000395.

52. Roseborough A, Ramirez J, Black SE, Edwards JD. Associations between amyloid β and white matter hyperintensities: a systematic review. Alzheimers Dement. 2017;13(10):1154–67. https://doi.org/10.1016/j.jalz.2017.01.026.

53. Toledo JB, Arnold SE, Raible K, et al. Contribution of cerebrovascular disease in autopsy confirmed neurodegenerative disease cases in the National Alzheimer's Coordinating Centre. Brain. 2013;136(Pt 9):2697–706. https://doi.org/10.1093/brain/awt188.

54. Mortamais M, Artero S, Ritchie K. Cerebral white matter hyperintensities in the prediction of cognitive decline and incident dementia. Int Rev Psychiatry. 2013;25(6):686–98. https://doi.org/10.3109/09540261.2013.838151.

55. Schmidt P. Bayesian Inference for Structured Additive Regression Models for Large-Scale Problems with Applications Tomedical Imaging: Dissertation an Der Fakultät Für Mathematik, Informatik Und Statistik Der Ludwig-Maximilians-Universität München. [Dissertation]: Ludwig-Maximilians-Universität München; 2017. http://nbn-resolving.de/urn:nbn:de:bvb:19-203731

56. Schmidt P. LST. A lesion segmentation tool for SPM. http://www.statistical-modelling.de/lst.html. Accessed 7 March 2022.

57. Bertens D, Tijms BM, Scheltens P, Teunissen CE, Visser PJ. Unbiased estimates of cerebrospinal fluid β-amyloid 1-42 cutoffs in a large memory clinic population. Alzheimers Res Ther. 2017;9(1):8. https://doi.org/10.1186/s13195-016-0233-7.

58. Schwarz G. Estimating the dimension of a model. Ann Stat. 1978;6(2). https://doi.org/10.1214/aos/1176344136.

59. Laboratory of Neuro Imaging, University of Southern California. ADNI: Alzheimer's Disease Neuroimaging Initiative. https://adni.loni.usc.edu/. Accessed 18 Dec 2022.

60. Hwang J, Jeong JH, Yoon SJ, et al. Clinical and biomarker characteristics according to clinical spectrum of Alzheimer's disease (AD) in the Validation Cohort of Korean Brain Aging Study for the Early Diagnosis and Prediction of AD. J Clin Med. 2019;8(3). https://doi.org/10.3390/jcm8030341.

61. Burnham SC, Coloma PM, Li Q-X, et al. Application of the NIA-AA Research Framework: towards a biological definition of Alzheimer's disease using cerebrospinal fluid biomarkers in the AIBL study. J Prev Alzheimers Dis. 2019;6(4):248–55. https://doi.org/10.14283/jpad.2019.25.

62. Grøntvedt GR, Lauridsen C, Berge G, et al. The amyloid, tau, and neurodegeneration (A/T/N) classification applied to a clinical research cohort with long-term follow-up. J Alzheimers Dis. 2020;74(3):829–37. https://doi.org/10.3233/JAD-191227.

63. Kakeda S, Korogi Y. The efficacy of a voxel-based morphometry on the analysis of imaging in schizophrenia, temporal lobe epilepsy, and Alzheimer's disease/mild cognitive impairment: a review. Neuroradiology. 2010;52(8):711–21. https://doi.org/10.1007/s00234-010-0717-2.

64. Karas GB, Scheltens P, Rombouts SA, et al. Global and local gray matter loss in mild cognitive impairment and Alzheimer's disease. Neuroimage. 2004;23(2):708–16. https://doi.org/10.1016/j.neuroimage.2004.07.006.

65. Chételat G, Landeau B, Eustache F, et al. Using voxel-based morphometry to map the structural changes associated with rapid conversion in MCI: a longitudinal MRI study. Neuroimage. 2005;27(4):934–46. https://doi.org/10.1016/j.neuroimage.2005.05.015.

66. Pini L, Pievani M, Bocchetta M, et al. Brain atrophy in Alzheimer's disease and aging. Ageing Res Rev. 2016;30:25–48. https://doi.org/10.1016/j.arr.2016.01.002.

67. Baron JC, Chételat G, Desgranges B, et al. In vivo mapping of gray matter loss with voxel-based morphometry in mild Alzheimer's disease. Neuroimage. 2001;14(2):298–309. https://doi.org/10.1006/nimg.2001.0848.

68. Bernardes R, da Silva FS, Oliveira Barbosa JH, Rondinoni C, et al. Neurodegeneration profile of Alzheimer's patients: a brain morphometry study. Neuroimage Clin. 2017;15:15–24. https://doi.org/10.1016/j.nicl.2017.04.001.

69. Zanchi D, Giannakopoulos P, Borgwardt S, Rodriguez C, Haller S. Hippocampal and amygdala gray matter loss in elderly controls with subtle cognitive decline. Front Aging Neurosci. 2017;9:50. https://doi.org/10.3389/fnagi.2017.00050.

70. Jones BF, Barnes J, Uylings HBM, et al. Differential regional atrophy of the cingulate gyrus in Alzheimer disease: a volumetric MRI study. Cereb Cortex. 2006;16(12):1701–8. https://doi.org/10.1093/cercor/bhj105.

71. Kumar D, Ganeshpurkar A, Kumar D, Modi G, Gupta SK, Singh SK. Secretase inhibitors for the treatment of Alzheimer's disease: Long road ahead. Eur J Med Chem. 2018;148:436–52. https://doi.org/10.1016/j.ejmech.2018.02.035.

72. van Dyck CH. Anti-amyloid-β monoclonal antibodies for Alzheimer's disease: pitfalls and promise. Biol Psychiatry. 2018;83(4):311–9. https://doi.org/10.1016/j.biopsych.2017.08.010.

73. Masliah E, Mallory M, Hansen L, Richard D, Alford M, Terry R. Synaptic and neuritic alterations during the progression of Alzheimer's disease. Neurosci Lett. 1994;174(1):67–72. https://doi.org/10.1016/0304-3940(94)90121-X.

74. Knowles RB, Gomez-Isla T, Hyman BT. Abeta associated neuropil changes: correlation with neuronal loss and dementia. J Neuropathol Exp Neurol. 1998;57(12):1122–30. https://doi.org/10.1097/00005072-199812000-00003.

75. Nation DA, Sweeney MD, Montagne A, et al. Blood-brain barrier breakdown is an early biomarker of human cognitive dysfunction. Nat Med. 2019;25(2):270–6. https://doi.org/10.1038/s41591-018-0297-y.

76. Buccellato FR, D'Anca M, Serpente M, Arighi A, Galimberti D. The role of glymphatic system in Alzheimer's and Parkinson's disease pathogenesis. Biomedicines. 2022;10(9). https://doi.org/10.3390/biomedicines10092261.

77. Fortea J, Vilaplana E, Alcolea D, et al. Cerebrospinal fluid β-amyloid and phospho-tau biomarker interactions affecting brain structure in preclinical Alzheimer disease. Ann Neurol. 2014;76(2):223–30. https://doi.org/10.1002/ana.24186.

78. Montal V, Vilaplana E, Alcolea D, et al. Cortical microstructural changes along the Alzheimer's disease continuum. Alzheimers Dementia. 2018;14(3):340–51. https://doi.org/10.1016/j.jalz.2017.09.013.

79. Stern Y, Arenaza-Urquijo EM, Bartrés-Faz D, et al. Whitepaper: Defining and investigating cognitive reserve, brain reserve, and brain maintenance. Alzheimers Dementia. 2020;16(9):1305–11. https://doi.org/10.1016/j.jalz.2018.07.219.

80. Ingala S, de Boer C, Masselink LA, et al. Application of the ATN classification scheme in a population without dementia: findings from the EPAD cohort. Alzheimers Dementia. 2021;17(7):1189–204. https://doi.org/10.1002/alz.12292.

81. Young AL, Oxtoby NP, Daga P, et al. A data-driven model of biomarker changes in sporadic Alzheimer's disease. Brain. 2014;137(Pt 9):2564–77. https://doi.org/10.1093/brain/awu176.

82. Firth NC, Primativo S, Brotherhood E, et al. Sequences of cognitive decline in typical Alzheimer's disease and posterior cortical atrophy estimated using a novel event-based model of disease progression. Alzheimers Dementia. 2020;16(7):965–73. https://doi.org/10.1002/alz.12083.

83. Nelson PT, Abner EL, Patel E, et al. The amygdala as a locus of pathologic misfolding in neurodegenerative diseases. J Neuropathol Exp Neurol. 2018;77(1):2–20. https://doi.org/10.1093/jnen/nlx099.

84. Mattsson-Carlgren N, Leuzy A, Janelidze S, et al. The implications of different approaches to define AT(N) in Alzheimer disease. Neurology. 2020;94(21):e2233–44. https://doi.org/10.1212/WNL.0000000000009485.

85. Illán-Gala I, Pegueroles J, Montal V, et al. Challenges associated with biomarker-based classification systems for Alzheimer's disease. Alzheimers Dement (Amst). 2018;10:346–57. https://doi.org/10.1016/j.dadm.2018.03.004.

Publisher's Note